Physical Chemistry and Chemical Physics

ARTICLE

Modulating the interaction between gold and TiO$_2$ nanowires for enhanced solar driven photoelectrocatalytic hydrogen generation

P. Sudhagar,[a‡*] Taeseup Song,[f‡] Anitha Devadoss,[a] Jung Woo Lee,[b] Marta Haro Remón,[c] Chiaki Terashima,[a] Volodymyr V. Lysak,[d] Juan Bisquert, Akira Fujishima[a], Sixto Gimenez,[c*] and Ungyu Paik[b*]

[5] The interaction strength of Au nanoparticles with pristine and nitrogen doped TiO$_2$ nanowire surface was analysed using density functional theory and their significance in enhancing the solar driven photoelectrocatalytic properties was elucidated. In this article, we prepared 4-dimethylaminopyridine capped Au nanoparticles decorated TiO$_2$ nanowires system. The density functional theory calculations

[10] show {101}facets of TiO$_2$ as the preferred phase for dimethylaminopyridine-Au nanoparticles anchoring with a binding energy of -8.282 kcal/mol. Besides, the interaction strength of Au nanoparticles was enhanced nearly four-fold (-35.559 kcal/mol) at {101} facets via nitrogen doping, which indeed amplified the Au nanoparticle density on nitrided TiO$_2$. The Au coated nitrogen doped TiO$_2$ (N-TiO$_2$-Au) hybrid electrodes show higher absorbance owing to the light scattering effect of Au nanoparticles. In addition,

[15] N-TiO$_2$-Au hybrid electrodes block the charge leakage from electrode to electrolyte and thus reduce the charge recombination at electrode/electrolyte interface. Despite the beneficial band narrowing effect of nitrogen in TiO$_2$ on the electrochemical and visible light activity in N-TiO$_2$-Au hybrid electrodes, it results low photocurrent generation at higher Au NPs loading (3.4×10^{-7} M) due to light blocking to N-TiO$_2$ surface. Strikingly, even with a ten-fold lower Au NPs loading (0.34×10^{-7} M), the synergistic effects

[20] of nitrogen doping and Au NPs on N-TiO$_2$-Au hybrid system yield high photocurrent compare to TiO$_2$ and TiO$_2$-Au electrodes. As a result, N-TiO$_2$-Au electrode produces nearly 270 μmol/hr cm^{-2} hydrogen, which is nearly two-fold higher than the pristine TiO$_2$ counterpart. The implications of these findings for the design of efficient hybrid photoelectrocatalytic electrodes are discussed.

Introduction

[25] Semiconductor photocatalysis and photoelectrochemistry, particularly involving TiO$_2$, is an influential field that plays an important role on environmental remediation and energy conversion applications. The striking features of TiO$_2$ including its high chemical stability in aqueous media, high photoactivity ,

[30] earth abundance and environmental benign nature, strongly encourage the use of this material as potential electron acceptor in light driven devices operating under solar radiation.[1, 2] The primary report on photoelectrocatalytic (PEC) water oxidation on TiO$_2$ by Fujishima and Honda,[3] has promoted a huge body

[35] literature on the design of nanostructured photocatalytic materials for realizing the solar driven PEC water oxidation process.[4, 5] Moreover, the photogenerated holes at the valence band of TiO$_2$ energetically favour the oxidation process of chemical components (like pollutants, etc.). This process can be understood

[40] as a renaissance of natural photosynthesis utilizing man-made materials. Nonetheless, the short wavelength cut-off property of TiO$_2$ permits accessing only a narrow segment (~5%) of the solar spectrum; resulting in low PEC efficiency.[6] Conversely, the VB edge position (~ 3.2 V vs NHE) of TiO$_2$ meets the energy

[45] requirement for successful PEC water oxidation, where most of the visible light band gap materials such as CdS, CdSe, GaAs, and GaP fall short.[7, 8] Therefore, developing strategies to amplify the light harvesting efficiency of TiO$_2$ (greater than 5%) without sacrificing their PEC water oxidation potential are strongly

[50] demanded to further improve the PEC performance of TiO$_2$.

In this context, gold nanoparticles (Au NPs) supported TiO$_2$ hybrid photocatalytic systems have attracted much attention because of their strong light absorption in the visible region, which arises from enhanced scattering and Localized Surface

[55] Plasmon Resonance (LSPR).[9-11] Due to LSPR, Au NPs can effectively harvest the electromagnetic energy of the incident light and concentrate it into "plasmonic hotspots", which in turn can maximize the local field intensity by a factor of 10^6.[12] Notably, one dimensional (1-D) TiO$_2$ nanostructures such as

[60] nanowires, nanotubes, nanofibers etc., afford ample room to accommodate the nanoparticles compared to their bulk counterparts.[13] Moreover, the rapid electron transport at 1-D TiO$_2$ crystallite framework is highly beneficial for the efficient charge collection at the relevant interfaces.[14, 15] In the case of TiO$_2$-Au

[65] hybrid photocatalytic systems, neither individual Au NPs nor TiO$_2$ can act as an efficient photocatalyst upon visible-light irradiation,[16] but a proper combination of both materials generates excellent visible-light PEC performances, even

significantly enhancing the UV photocatalysis of TiO_2.[17-21] This indicates that the interfacial interaction between Au NPs and TiO_2 plays a key role on achieving optimum PEC performance.

So far, a number of strategies have been documented in literature for anchoring the Au NPs on TiO_2 surfaces. For instance, Au NPs were coated on TiO_2 *via* physical evaporation or sputtering resulted in the formation of inhomogenous NPs coating on the metal oxide host surface.[22, 23] Alternatively, it has been reported that Au NPs can also be deposited on TiO_2 substrates *via* directly reducing gold salts by chemical reduction or photodeposition.[24, 25, 26, 27, 28] Unfortunately, such deposition techniques affect the supporting semiconductors due to the multiple post-treatment steps. Similarly, controlling the size, shape and distribution of Au NPs using such approaches still remain challenging. Recently, we have demonstrated a straightforward method of anchoring 4-dimethylaminopyridine (DMAP) capped Au NPs on TiO_2 hollow nanowires, which in turn resulted in enhanced photocatalytic performance towards dye degradation.[29] In the present study, we investigate the underlying mechanism behind the single-step anchoring of DMAP capped Au NPs on TiO_2 nanowires and their respective interactions were studied using theoretical simulations based on first principle theory. The interaction between DMAP capped Au NPs and TiO_2 nanowires were modulated via nitrogen doping the TiO_2. The influence of nitrogen doping and DMAP capped Au NPs anchoring on TiO_2 band modification was elucidated. The finite-difference time domain (FDTD) method was used to quantitatively analyse the electromagnetic field enhancement in TiO_2-Au hybrid photocatalytic system. Our theoretical and experimental results demonstrate the synergistic effect of Au NPs (visible light scattering) and nitrogen doping (band gap narrowing effect) on PEC water oxidation process and the implications of these findings are discussed.

Experimental

Materials

All materials were received from Sigma-Aldrich and used as received.

Fabrication of TiO_2 Nanowires Array

Vertically aligned TiO_2 hollow nanowires onto FTO substrates were grown using ZnO nanorod array templates. First step, ZnO film of 200 nm was deposited on FTO substrate using radio frequency magnetron sputtering. Followed that, the ZnO seed layer coated FTO substrate was immersed into aqueous solution of 0.025 M zinc nitrate hexahydrate and 0.025 M hexamethylenetetramine and the sample was kept at 85 ° C for 10 h for the growth of vertically aligned ZnO nanorods array. After ZnO nanorods growth, the substrates were rinsed with deionized water.

In the second step, TiO_2 layer will be grown on ZnO nanorod array as follows: the resultant ZnO NR array template was kept at aqueous solution of 0.075 M ammonium hexafluorotitanate and 0.2 M boric acid. This chemical bath deposition results thin layer of TiO_2 coating ZnO nanorods. Subsequently, the TiO_2 coated ZnO electrode is immersed in a 0.5 M boric acid solution for 1 h and the ZnO template is removed and rinsed with deionized water. Finally, vertically aligned TiO_2 NWs arrays are obtained. The TiO_2 NWs samples were calcined at 500 ° C for 0.5 h under Ar atmosphere..

For nitridation onto TiO_2 NW, the electrodes were transferred to a chemical vapour deposition (CVD) chamber. The nitridation process was carried out at 500 ºC with H_2 and NH_3 with flow rates of 50–200 standard cubic centimetre per minute (sccm) and 100–300 sccm, respectively.

Synthesis of Au NPs

DMAP-capped Au NPs were synesized using the phase transfer procedure.[30] Briefly, 0.030 M aqueous solution of $HAuCl_4.3H_2O$ was added to 0.025 M tetraoctylammonium bromide (TOAB) in toluene. Then, 0.4 M aqueous $NaBH_4$ was added drop-wise to the mixture with stirring, causing an immediate reduction to occur. After 24 h, the two phases were separated and the toluene phase was subsequently washed with 0.1 M H_2SO_4, 0.1 M NaOH, and H_2O (three times), and then dried over anhydrous Na_2SO_4. An equal volume of 0.1 M aqueous solution of DMAP was then added. The phase transfer is clearly visible as the dark pink coloured solution transfers from toluene to water due to the addition of the DMAP and was completed within 1 h. Assuming a 100% efficient reduction of gold chloride and no losses during transfer and washing steps, the particle size yields a particle concentration of approximately 6.8×10^{-7} M in the stock solution arising from the nanoparticle synthesis.

Assembly of Au NPs on TiO_2 Nanowires Array

Au NPs coating on TiO_2 and N-TiO_2 NWs arrays was obtained by immersing the TiO_2 electrodes in positively charged, water soluble DMAP-capped Au NPs solution (3.4×10^{-7} M) for 5 min. The positively charged DMAP-capped Au NPs were attracted towards the negatively charged surface of TiO_2 NWs and N-TiO_2 NWs, resulting in the facile formation of electrostatically assembled TiO_2-Au and N-TiO_2-Au hybrid photocatalytic electrodes. After Au NPs coating on these electrodes DMAP molecules were removed by sintering process.

Theoretical calculations

The energy calculations were performed with PW91 method generalized gradient approximation (GGA) and plane wave model using CASTEP program. The supercell of 20 Å×20 Å × c was used for the calculation, which represents nanowires length along the tube axis as c. All atoms were described using Vanderbilt ultrasoft pseudopotentials and cut off energy of 240 eV where the set of k-points used to expand the electronic wave function based on the Monkhorst-Pack scheme within 5.0×10^{-5} eV atom^{-1} of total energies convergence. Electron density was investigated with optimized geometries. The binding energies of atoms on the nanotubes were calculated by equation (1)

$$E_b = E_{nanotube+atom} - (E_{nanotube} + E_{atom}). \quad (1)$$

Structural, and optical characterization

The surface of various TiO_2 nanowires array was characterized using a field emission scanning electron microscope (FE-SEM, JEM-3100F, Jeol, Tokyo, Japan) and a field emission transmission electron microscope (FE-TEM, JSM 7600F, JEOL, Tokyo, Japan). The chemical environment of pure and N doped TiO_2 electrodes were analyzed by x-ray photoelectron spectroscopy (XPS) using an angular resolved electron analyzer
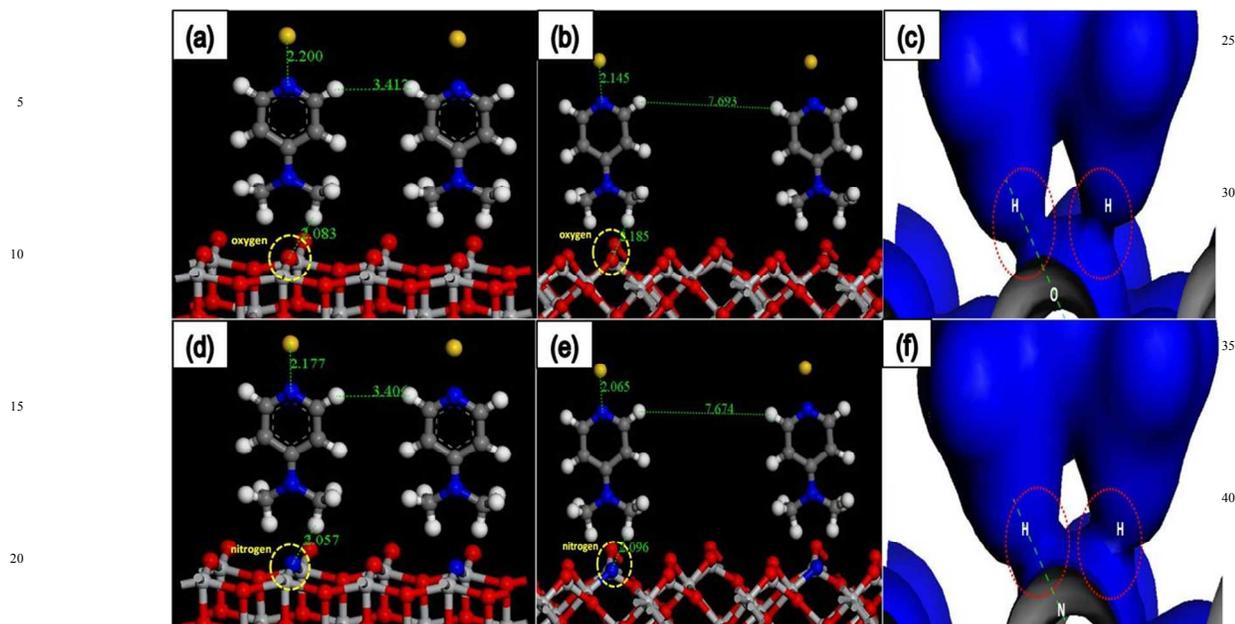
with a monochromated Al Kα source (Theta Probe, Thermo

Figure 1: The optimal orientations of TiO_2 (a, b) and N-TiO_2 (d, e) surface illustrating the binding mechanism of DMAP-Au NPs at {001} and {101} planes, respectively. The electron density distribution estimated at TiO_2-Au (c) and N-TiO_2-Au (f) electrodes.

Fisher Scientific). The optical diffuse reflectance spectra of the electrodes were recorded in the range of 350–900 nm using a V670 JASCO UV-Vis spectrophotometer. The absorbance of the electrodes was estimated from diffuse reflectance measurements (R) directly using the Kulbelka-Munk relation, $F.R. = (1-R)^2/2R$ with in build software from JASCO UV-Vis spectrometer. We have assumed that the scattering term is similar for photoelectrodes with and without Au loading.

(Photo)- electrochemical characterization

The (photo)-electrochemical analysis was done using a three electrode configuration. The as-prepared TiO_2, TiO_2-Au, N-TiO_2 and N-TiO_2-Au electrodes (electrode area 1 cm^2) were used as the working electrode, Ag/AgCl as the reference and Pt foil as the counter electrode. 0.5 M of Na_2SO_4 (Sigma Aldrich) (pH=6.1) was used as the electrolyte for all PEC measurements without any additional additives. Cyclic voltammograms were recorded using the advanced potentiostat (PGSTAT-30 from Autolab) with the scanning rate 50 mV/s. The photocurrent measurements were recorded using a solar simulator with a 300 W xenon arc-lamp (Hayashi- LA 251-Xe). The light intensity was calibrated using a silicon photodiode (100 mWcm^{-2}). The electrolyte was bubbled with nitrogen gas for 30 min to avoid the presence of oxygen (electron acceptor) in the solution. The IPCE measurements were carried out by employing a 300 W Xe lamp coupled to a computer-controlled monochromator; the photoelectrode was polarized at the desired voltage (1.6 V vs RHE) with a Gamry potentiostat, and the photocurrent was measured using an optical power meter 70310 from Oriel Instruments. A Si photodiode was used to measure the light intensity to calibrate the system. The output gas samples were collected from the head space of a

sealed PEC chamber using an air-tight gas syringe through the manual sampling port in the top of the chamber (flexible cork made of Teflon) and further subjected to gas chromatographic analysis to evaluate the constituents of the gas products.

Theoretical calculations

To get insights into the binding mechanism of positively charged DMAP-capped Au NPs on TiO_2 NWs and N-TiO_2 NWs, it is important to estimate the binding energies in the hybrid systems. First principles based simulations provide direct evidence of interaction energies between DMAP-Au NPs and TiO_2 semiconductor, which can be used to detect the optimal binding sites and to predict the maximal affinity that a nanoparticle could attain from them. The binding characteristics in TiO_2-Au and N-TiO_2-Au hybrid photocatalytic systems were analyzed using first principles theory. Firstly, the binding energies between molecular DMAP and Au were estimated. It was found that the DMAP molecule strongly binds to gold with - 14.01 kcal/mol binding energy, which could be ascribed to the high binding affinity of Au atoms towards the pyridine moieties in DMAP.

Recent studies show that the photocatalytic activity of TiO_2 strongly depends on their crystal facets.[31-33] Moreover, it was realized that deposition of metal nanoparticles (Ag, Au and Pt) onto selective {101} facets of anatase TiO_2 crystals with different percentages of exposed {001} and {101} facets can effectively enhance the photocatalytic activity of TiO_2 in both photoreduction and photo-oxidation processes.[34, 35] In this line, we examined the binding nature of DMAP-Au NPs on {101} and {001} facets of TiO_2. Figure 1 shows the optimal binding sites of DMAP-Au NPs on (a) {001} facets and (b) {101} facets of TiO_2. The {101} facet of TiO_2 shows higher binding energy (-8.282

kcal/mol) towards DMAP-Au NPs anchoring compared to the {001} facets of TiO$_2$ (-6.48 kcal/mol), illustrating the higher affinity of {101} surfaces towards DMAP-Au NPs anchoring. Figure 1c shows the density of electron cloud at TiO$_2$-Au hybrid electrode.

The reported excellent catalytic activity and band structure modifications of TiO$_2$ upon nitrogen doping[36-39] inspired us to investigate the effect of nitrogen doping on DMAP-Au NPs binding. Figure 1 (d-f) shows the binding orientations and density of electron cloud distribution in N-TiO$_2$-Au hybrid electrodes. As anticipated, higher binding energies (-8.86 kcal/mol) were observed for DMAP-Au NPs anchoring on N-TiO$_2$ than on pristine TiO$_2$ NWs (-6.48 kcal/mol) at {001} surface. This could be ascribed to the higher binding affinity of pyridines and Au towards nitrogen. Strikingly, the binding energies were found to be remarkably enhanced at the {101} surface of N-TiO$_2$ NWs. The N-TiO$_2$-Au hybrid system shows a binding energy of -35.56 kcal/mol at {101} surface, which is nearly four times higher than that observed for {001} plane of N-TiO$_2$ NW. This strongly suggests that the Au NPs can be effectively coated onto N-TiO$_2$ by electrostatic attraction.
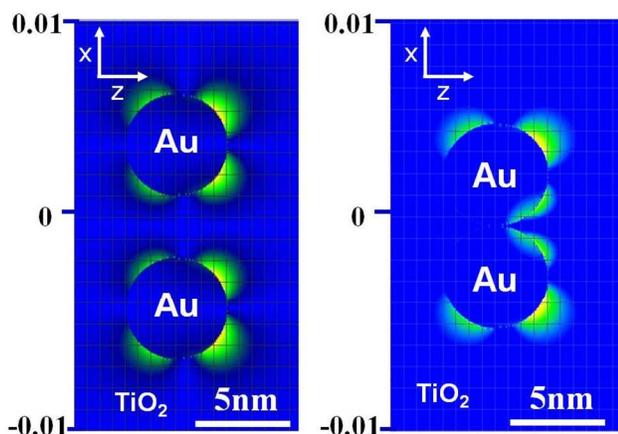

Figure 2. Spatial distribution of electric-field energy density of TiO$_2$-Au hybrid photocatalytic system at different spacing conditions: (a) with few nm spacing and (b) Au nanoparticles in contact (y axis indicated the distance in nm).

On the other hand, in view of improving the light harvesting efficiency of TiO$_2$, Au NPs decoration found to improve the visible light activity of hybrid materials owing to their strong scattering effect and enhanced absorption around 520 nm due to LSPR band. To understand the origin and the extent of improved visible light activity in TiO$_2$-Au hybrid systems, the light scattering effect of Au NPs at TiO$_2$ NWs was further analyzed using finite-difference time-domain (FDTD). Fig.2 shows the electric field (E-field) distribution in the perpendicular direction, across the Au NPs at TiO$_2$-NWs surface obtained from FDTD simulations. The permittivity of gold was analyzed using Lorenz-Drude dispersive model.[40]

$$\varepsilon_r(\omega) = \varepsilon_{r,\infty} + \sum_{m=0}^{5} \frac{G_m \Omega_m^2}{\omega_m^2 - \omega^2 + j\omega\Gamma_m} \qquad (1)$$

where, $\varepsilon_r(\omega)$ is the relative permittivity at infinity frequency, G_m

is the strength of each resonance term, Ω_m is the plasma frequency, ω and ω_m is the angular and resonant frequency, respectively, and Γ_m is the damping factor or collision frequency. Fig. 2(a) and (b), clearly illustrate the electric field generation around the Au NPs. The electric field extension varies with Au NPs loading (spacing) on TiO$_2$. The visible light scattering centres around Au NPs transformed the light reception at TiO$_2$. However, higher loadings of Au NPs on TiO$_2$ found to scatter the major portion of input light, which may reduce the light transmission reaching the TiO$_2$ surface. Thus, it is anticipated that TiO$_2$-Au hybrid system benefits not only from improved LSPR band facilitated absorption at 520 nm, but also from the light scattering effect of Au NPs, which could effectively improve the light absorption properties of TiO$_2$ itself.

Experimental results

From the above discussion, it is inferred that the Au NPs decoration at TiO$_2$ NWs could yield high PEC energy conversion efficiency, mainly through light scattering and co-catalyst effect. Moreover, nitrogen doping was found to enhance the interaction between Au NPs and TiO$_2$ as well as enhancing the visible light activity of TiO$_2$ by band gap narrowing effect.[39] In order to understand the role of Au NPs decoration and nitrogen doping, we have designed and fabricated Au NPs decorated TiO$_2$ NWs and N-TiO$_2$ NWs arrays onto fluorinated tin oxide (FTO) substrates. Figure 3 shows the electron microscopy images of nitrided TiO$_2$ (N-TiO$_2$) NWs, Au NPs coated TiO$_2$ NWs (TiO$_2$-Au) and N-TiO$_2$ NWs (N-TiO$_2$-Au) arrays, respectively.
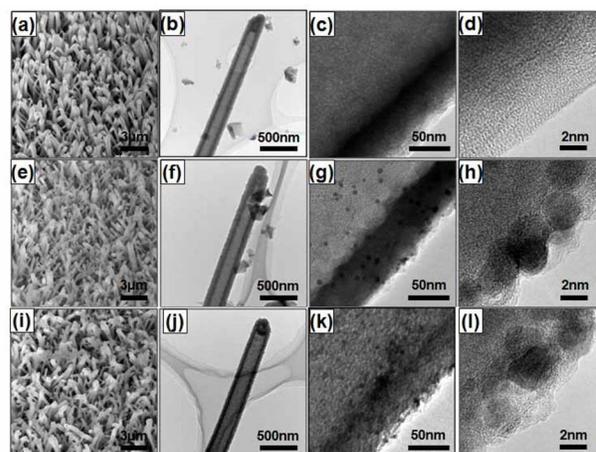

Figure 3. (a), (e) and (i) SEM and images of N-TiO$_2$, TiO$_2$-Au and N-TiO$_2$-Au electrodes, respectively. Corresponding TEM images were presented in right hand side of each sample.

Scanning electron microscopy (SEM) and transmission electron microscopy (TEM) images of N-TiO$_2$ NWs clearly reveal their vertically aligned geometry and 1-D structure (Fig. 3a). The N-TiO$_2$ NWs have a length of ~5 μm, inner free space of ~200 nm and shell thickness of ~50 nm, respectively (Fig. 3b). From Fig. 3c and 3d, a thin amorphous layer is observed on TiO$_2$. This layer represents the formation of TiN/TiO$_x$N$_y$ on TiO$_2$ NW surface during the nitridation process. Although it was difficult to obtain lattice resolved TEM images at the surface of N-TiO$_2$ NWs, the X-ray diffraction (XRD) and SAED patterns support that N-TiO$_2$

NWs maintain their polycrystalline anatase phase (**See Supporting information Fig.S1**). There are no noticeable changes on the geometry of the NWs after Au NPs anchoring (Fig. 3f & Fig. 3j). Au NPs with an average diameter of ~ 5 nm

5 were observed in the high magnification TEM images (Fig. 3(i)) (also **See Supporting information Fig.S2**). These images (Fig. 3h & Fig. 3l) confirm the higher loading of Au NPs on N-TiO$_2$ NWs compared to pristine TiO$_2$ NWs.
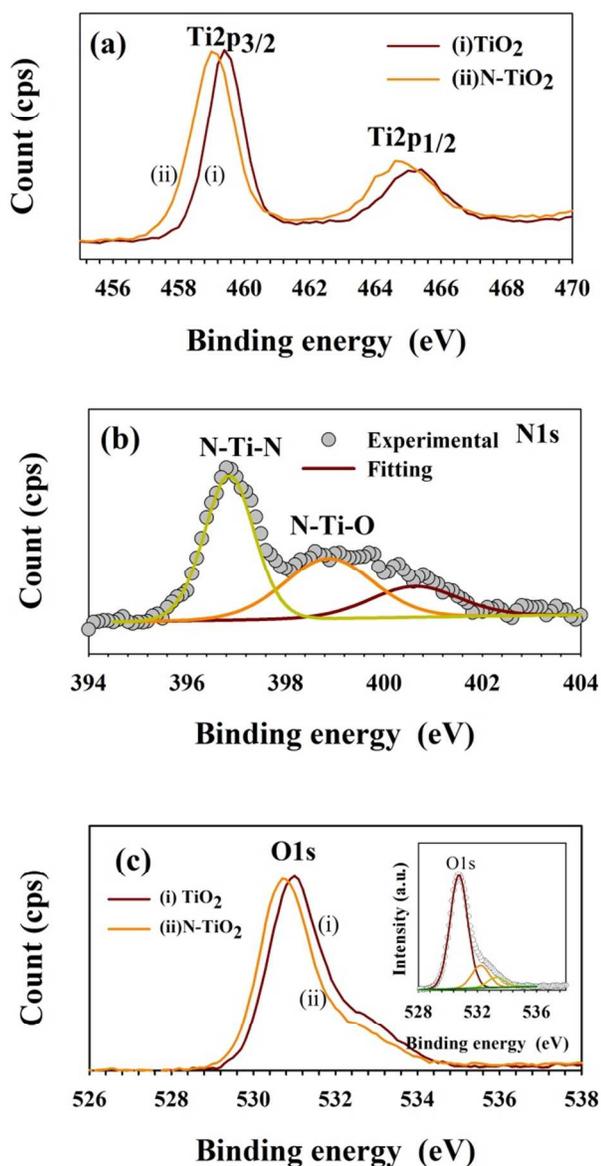
10 **Figure 4.** XPS results of (a) Ti 2p (b) N1S and (c) O1s core spectra of TiO$_2$ and N-TiO$_2$ electrodes.

The effect of nitrogen doping on TiO$_2$ NWs was studied with X ray photoelectron spectroscopy. Fig. 4 (a) shows the core spectra of Ti 2p in pristine TiO$_2$ NWs and N-TiO$_2$ NWs. The shoulder

15 peaks at 459.4 eV and 465.1 eV correspond to Ti2p$_{3/2}$ and Ti2p$_{1/2}$, respectively.[41] In N-TiO$_2$ NWs, these peaks were shifted toward lower binding energy indicating the successful nitrogen doping at the TiO$_2$ NWs. Further examining the N1s core spectra (Fig. 4b), the peaks at 396.8, 398.8, and 400.6 eV provide a clear picture of

20 nitrogen environment at TiO$_2$ NWs. The peak at 396.8 eV is attributed to the existence of atomic β-N at TiO$_2$ matrix and the peak at 398.8 eV implies the substitution of O$_2^-$ by nitrogen ions and thus, results in the formation of N-Ti-O.[42, 43] This confirms the existence of Ti^{3+} due to the incorporation of nitrogen atoms

25 into oxygen lattice sites. The weaker peak at 400.6 eV indicates the interstitial doping which induces an additional impurity state above the valence band of TiO$_2$.[44] The atomic ratio of nitrogen doping carriers was estimated from Fig. 4(b) and found to be 5.8 wt%. The broad features of O1s peak in Fig.4c were

30 deconvoluted with Gaussian fit (Fig.4c inset). Three distinct peaks were observed at 530.9, 532.2 and 533.2 eV representing the lattice oxygen, surface hydroxyl oxygen and surface adsorbed oxygen, respectively. The atomic weight of lattice oxygen at TiO$_2$ NWs was estimated to be 51.5%, which was reduced to 47.6%

35 upon nitrogen doping. This indicates the possibility of nitrogen atoms occupying the oxygen vacancies. The influence of nitrogen doping on the work function of TiO$_2$ NWs was examined using ultraviolet photoelectron spectroscopy (**See supporting information Fig.S3**). The valence band maximum (VBM)

40 position of TiO$_2$ NWs at ~3.26 eV was shifted to ~2.69 eV upon nitrogen doping. This indicates that nitrogen doping carriers are creating sub-bands or defects above the VB of TiO$_2$ as discussed in the XPS results.
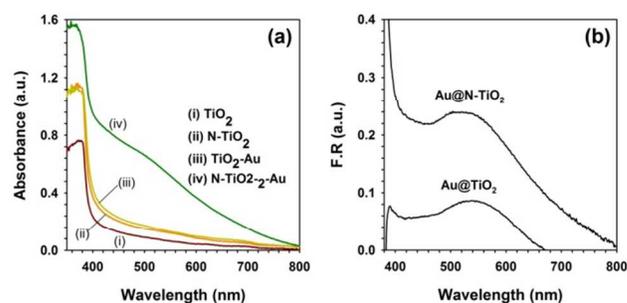
45 **Figure 5.** Absorbance spectra of TiO$_2$ and N-TiO$_2$ electrodes in the presence and absence of Au NPs; (b) Kulbelka-Munk relation of Au NPs decorated at TiO$_2$ NWs and N-TiO$_2$ NWs).

In order to study the contribution of DMAP-Au NPs towards the visible light activity of TiO$_2$-Au and N-TiO$_2$-Au hybrid

50 photocatalysts, diffuse reflectance measurements were performed. The results are showed in Fig. 5a. The Kulbelka-Munk absorbance contribution of TiO$_2$ NWs and N-TiO$_2$ NWs was subtracted from the absorbance spectrum of TiO$_2$-Au and N-TiO$_2$-Au hybrids, respectively (inset of Figure 5). Both spectra

55 confirm the enhanced scattering induced by the presence of Au NPs, being the LSPR effect negligible for these specimens. Although, Au NPs coating at TiO$_2$ and N-TiO$_2$ was carried out at identical condition, N-TiO$_2$-Au hybrid electrodes showed higher absorbance, indicating higher loading of Au NPs in good

60 correspondence with the TEM measurements (Fig. 2h & 2l) and Kulbelka-Munk function (F.R.) (inset of Figure 5). This is attributed to the higher binding energy observed at the N-TiO$_2$ surfaces. The broad absorption nature of N-TiO$_2$-Au may be originated from the light scattering effect which amplifies the

65 absorbance of TiO$_2$.[45]

To test the photoelectrochemical (PEC) water oxidation performance, we measured J-V characteristics of these electrodes in the dark and upon illumination conditions. From Fig. 6(a), it was found that TiO$_2$-Au hybrid electrode showed four times higher photocurrent ~0.4 mAcm^{-2} than pristine TiO$_2$ NWs electrode (0.11 mAcm^{-2}). This photocurrent enhancement may be due to the combined effect of higher optical absorption due to scattering and co-catalytic effect of Au NPs in water oxidation through the formation of Au/TiO$_2$ Schottky junction.[46, 47] In addition, it may facilitate the charge separation at TiO$_2$/electrolyte interfaces and thus reduces the recombination of electrons through surface states of TiO$_2$.[48] In the case of nitrogen doping at TiO$_2$ NWs, the photocurrent density was slightly enhanced (0.22 mAcm^{-2}), which might be ascribed to the promotion of visible light activity of TiO$_2$ through band gap narrowing effect (**See supporting information S3 and S4**).

In striking contrast, the photocurrent at N-TiO$_2$-Au hybrid system was only slightly higher than N-TiO$_2$ NWs system. This might be due to excessive Au NPs decoration (From Fig.3 (l)), which may result in forward light scattering blocking the light photons reaching N-TiO$_2$ NWs surface and also reduce the interfacial contact between N-TiO$_2$ and FTO electrode, thus hindering the photoholes participating in the water oxidation process.[18] This implies that there exist a trade-off between the enhanced light scattering due to Au NPs decoration and visible light photons reception at N-TiO$_2$ NWs, which necessitates the optimization of Au NPs loading onto N-TiO$_2$ NWs. We have recently reported that the photoelectrochemical performance of TiO$_2$/Au nanocomposites has a volcano dependence with Au loading.[28]
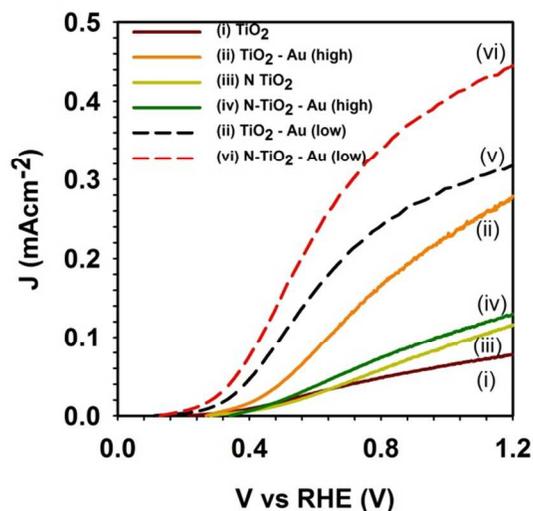

Figure 6. J-V results of PEC water splitting using different photoanode electrodes. Note that two different Au concentrations were used for decorating working electrodes: low – 0.34×10^{-7} M; high- 3.4 x 10^{-7} M).

Interestingly, the Au NPs decorated TiO$_2$ and N-TiO$_2$ electrodes using low concentration stock solution (0.34×10^{-7} M), here referred as TiO$_2$-Au (low) and N-TiO$_2$-Au (low), respectively lead to higher photocurrent compared to the high Au concentration samples, as observed in Figure 6. This photocurrent enhancement strongly suggests minimizing the optical blocking effect through control the Au NPs loading on N-TiO$_2$.

Furthermore, the stability of electrodes in photocurrent generation is examined with chronoamperometric curves (**See supporting information S5**). The significant decrease of the photocurrent in both TiO$_2$ and TiO$_2$-Au electrodes may be attributed to the current leakage at TiO$_2$/FTO interfaces to electrolyte through naked FTO surface (uncovered TiO$_2$ area). Another plausible reason may arise from Au stability under long time photo-irradiation. However it is not clear at this moment and further research on this topic in needed. It is anticipated that inserting compact TiO$_2$ blocking layer between TiO$_2$ and FTO layers will hinder the electron flow from the charge collector to electrolyte.

In order to further corroborate the absence of plasmonic effect at Au coated TiO$_2$ electrodes, we recorded IPCE spectra (**See supporting information Fig. S6**). There is no photocurrent peak exhibit around 550 nm in TiO$_2$-Au electrode as observed in optical absorption spectra (Figure 5b). This implies that there is no electron injection from Au nanoparticles to TiO$_2$ by plasmonic effect. Instead, Au NPs are promoting the optical absorption of TiO$_2$ through scattering effect. In addition, Au NPs play a critical role as co-catalyst in water oxidation process as scheduled in Figure S4. The photoholes generated at the valence band of TiO$_2$ and N-TiO$_2$ is injected into Au NPs and may oxidize the water molecules into oxygen and protons.

Aiming at the technological exploitation of the photocurrent enhancement due to nitrogen doping and loading of Au nanoparticles, we carried out the deposition of these structures on flexible stainless steel (SS) substrates. The flexible photoelectrodes are highly promising in solar-to hydrogen fuel production owing to their lower weight and cost, compared to FTO, together with more versatile mechanical properties. However, the TiO$_2$ nanowire fabrication onto flexible SS substrates remains challenging. Similar deposition procedure of TiO$_2$ on FTO substrates explained in the experimental session was repeated for fabricating TiO$_2$ NW on flexible SS substrates. We adopt the optimized Au NPs concentration condition (0.34×10^{-7} M) from the Figure 6, and reconstructed the TiO$_2$-Au hybrid systems onto flexible stainless steel (SS) substrates instead of FTO substrates (sample photo presented in inset of Figure 7).

The *j-v* characteristics of Au-TiO$_2$-SS and Au-N-TiO$_2$-SS electrodes were tested in 0.5M Na$_2$SO$_4$ aqueous electrolyte with three electrode PEC cell step up. The *j-v* characteristic of N-TiO$_2$-Au-SS is displayed in Figure 7 (a). The higher photocurrent density achieved in N-TiO$_2$-Au compared to TiO$_2$-Au electrode agrees well with the trends presented in Figure 6. The scattering effect by Au NPs, band gap narrowing effect by N doping and catalysis at optimal concentration leads to high photocurrent generation at the Au-N-TiO$_2$-SS sample. A small onset potential shift occurred in this sample towards negative potential region, also in good agreement with results showed in Figure 6. We believe that this cathodic shift can be related to enhanced charge collection at the contact for the N-doped TiO$_2$.
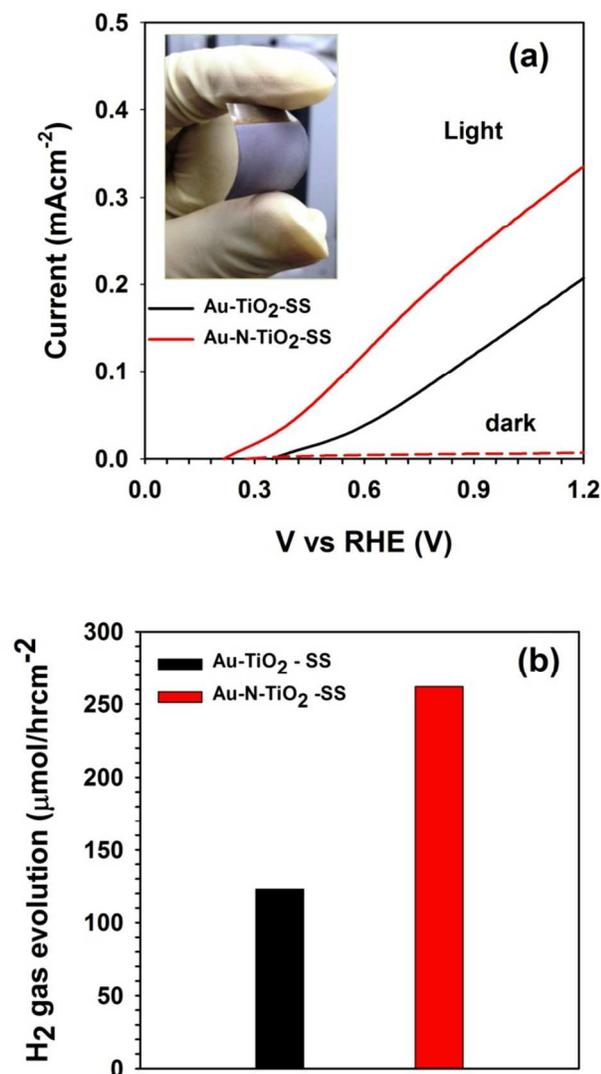
Figure 7. (a) J-V characteristics of PEC water splitting with different photoanodes (inset: photograph of $N-TiO_2$-Au on flexible SS substrate)(b) hydrogen gas evolution from PEC experiments using different photoanodes.

The gas evolution from PEC water oxidation experiment was collected for one hour under light illumination at 1 V vs RHE potential, and analysed using gas chromatography (Fig. 7b). It is observed that TiO_2-Au hybrid electrodes could generate hydrogen of about 120 μmol/hr cm^{-2}. Interestingly, the hydrogen generated at $N-TiO_2$-Au hybrid electrodes was about 270 μmol/hr cm^{-2}. The described bendable architecture of $N-TiO_2$-Au on SS substrates (inset of Fig. 7a) with light weight and low cost can be beneficial in large scale flexible PEC fuel generation.[49, 50] Another advantage of both side conducting nature of SS substrates enable us to design an artificial leaf based (back side coated with electrocatalyst) on monolithic wireless type solar fuel cells.[51]

Conclusions

Hybrid photocatalytic systems developed by anchoring DMAP-Au NPs on $N-TiO_2$ nanowires exhibit interesting optical and photocatalytic properties for water oxidation. Nitrogen doping of TiO_2 both maximizes the DMAP-Au NPs loading and improves the optical absorption due to band narrowing effect. DMAP-Au NPs anchoring amplifies the visible light activity of TiO_2 and $N-TiO_2$ via light scattering effect and also, improves the charge recombination at electrode/electrolyte interface. After optimization of the Au loading on the nanostructured photoelectrodes, N-doped TiO_2 leads to enhanced photocurrent generation and slightly more favourable onset potential on both FTO and SS substrates. Hydrogen generation measured on films deposited on flexible SS substrates was significantly higher on N-doped TiO_2 nanostructures.

Notes and references

[a] *Photocatalysis International Research Center, Research Institute for Science & Technology, Tokyo University of Science, 2641 Yamazaki, Noda, Chiba 278-8510, Japan,; E-mail: vedichi@gmail.com*
[b] *Department of Energy Engineering and Advanced Materials Science Engineering, Hanyang University, Seoul 133 791, South Korea; E-mail: upaik@hanyang.ac.kr*
[c] *Photovoltaic and Optoelectronic Devices Group, Departament de Física, Universitat Jaume I, 12071 Castelló, Spain; E-mail: sjulia@uji.es*
[d] *Department of Nanotechnology and Material Science, National Research University of Information Technologies, Mechanics and Optics, Saint Petersburg, Russia*
[e] *Department of Chemistry, Faculty of Science, King Abdulaziz University, Jeddah, Saudi Arabia*
[f] *School of Materials Science and Engineering, Yeungnam University, Gyeongsan 712-749, Korea*

† Electronic Supplementary Information (ESI) available: [XRD, UPS and impedance results]. See DOI: 10.1039/b000000x/
‡ These authors equally contributed to the research.

1. A. L. Linsebigler, G. Lu and J. T. Yates, *Chemical Reviews*, 1995, 95, 735-758.
2. P. V. Kamat, *The Journal of Physical Chemistry C*, 2012, 116, 11849-11851.
3. A. Fujishima and K. Honda, *Nature*, 1972, 238, 37-38.
4. M. A. Fox and M. T. Dulay, *Chemical Reviews*, 1993, 93, 341-357.
5. A. Kudo and Y. Miseki, *Chemical Society Reviews*, 2009, 38, 253-278.
6. S. U. M. Khan, M. Al-Shahry and W. B. Ingler, *Science*, 2002, 297, 2243-2245.
7. M. Gratzel, *Nature*, 2001, 414, 338-344.
8. L. Yang, H. Zhou, T. Fan and D. Zhang, *Physical Chemistry Chemical Physics*, 2014, 16, 6810-6826.

Physical Chemistry Chemical Physics Accepted Manuscript

9. D. Pile, *Nat Photon*, 2013, 7, 3-3.

10. S. Linic, P. Christopher and D. B. Ingram, *Nat Mater*, 2011, 10, 911-921.

11. P. Christopher, H. Xin, A. Marimuthu and S. Linic, *Nat Mater*, 2012, 11, 1044-1050.

12. C. Clavero, *Nat Photon*, 2014, 8, 95-103.

13. P. Rodenas, T. Song, P. Sudhagar, G. Marzari, H. Han, L. Badia-Bou, S. Gimenez, F. Fabregat-Santiago, I. Mora-Sero, J. Bisquert, U. Paik and Y. S. Kang, *Advanced Energy Materials*, 2013, 3, 176-182.

14. P. Sudhagar, V. Gonzalez-Pedro, I. Mora-Sero, F. Fabregat-Santiago, J. Bisquert and Y. S. Kang, *Journal of Materials Chemistry*, 2012, 22, 14228-14235.

15. H. Han, P. Sudhagar, T. Song, Y. Jeon, I. Mora-Sero, F. Fabregat-Santiago, J. Bisquert, Y. S. Kang and U. Paik, *Chemical Communications*, 2013, 49, 2810-2812.

16. J.-J. Chen, J. C. S. Wu, P. C. Wu and D. P. Tsai, *The Journal of Physical Chemistry C*, 2010, 115, 210-216.

17. Z. W. Seh, S. Liu, M. Low, S.-Y. Zhang, Z. Liu, A. Mlayah and M.-Y. Han, *Advanced Materials*, 2012, 24, 2310-2314.

18. Y.-C. Pu, G. Wang, K.-D. Chang, Y. Ling, Y.-K. Lin, B. C. Fitzmorris, C.-M. Liu, X. Lu, Y. Tong, J. Z. Zhang, Y.-J. Hsu and Y. Li, *Nano Letters*, 2013, 13, 3817-3823.

19. K. Kim, P. Thiyagarajan, H.-J. Ahn, S.-I. Kim and J.-H. Jang, *Nanoscale*, 2013, 5, 6254-6260.

20. M. A. Nadeem, M. Murdoch, G. I. N. Waterhouse, J. B. Metson, M. A. Keane, J. Llorca and H. Idriss, *Journal of Photochemistry and Photobiology A: Chemistry*, 2010, 216, 250-255.

21. Z. Zhang, L. Zhang, M. N. Hedhili, H. Zhang and P. Wang, *Nano Letters*, 2012, 13, 14-20.

22. V. S. K. Chakravadhanula, C. Kübel, T. Hrkac, V. Zaporojtchenko, T. Strunskus, F. Faupel and L. Kienle, *Nanotechnology*, 2012, 23, 495701.

23. F. Liu, C. Tang, Z. Wang, C. Sui and H. Ma, *Nanotechnology*, 2014, 25, 125703.

24. J. A. Ortega Méndez, C. R. López, E. Pulido Melián, O. González Díaz, J. M. Doña Rodríguez, D. Fernández Hevia and M. Macías, *Applied Catalysis B: Environmental*, 2014, 147, 439-452.

25. Y.-F. Yang, P. Sangeetha and Y.-W. Chen, *International Journal of Hydrogen Energy*, 2009, 34, 8912-8920.

26. A. Tanaka, S. Sakaguchi, K. Hashimoto and H. Kominami, *Catalysis Science & Technology*, 2014, 4, 1931-1938.

27. E. Pedrueza, J. L. Valdés, V. Chirvony, R. Abargues, J. Hernández-Saz, M. Herrera, S. I. Molina and J. P. Martínez-Pastor, *Advanced Functional Materials*, 2011, 21, 3502-3507.

28. M. Haro, R. Abargues, I. Herraiz-Cardona, J. Martínez-Pastor and S. Giménez, *Electrochimica Acta*, 2014, 144, 64-70.

29. P. Sudhagar, A. Devadoss, T. Song, P. Lakshmipathiraj, H. Han, V. V. Lysak, C. Terashima, K. Nakata, A. Fujishima, U. Paik and Y. S. Kang, *Physical Chemistry Chemical Physics*, 2014, DOI: 10.1039/c4cp02009j.

30. A. Devadoss, P. Sudhagar, S. Das, S. Y. Lee, C. Terashima, K. Nakata, A. Fujishima, W. Choi, Y. S. Kang and U. Paik, *ACS Applied Materials & Interfaces*, 2014, 6, 4864-4871.

31. P. A. Morris Hotsenpiller, J. D. Bolt, W. E. Farneth, J. B. Lowekamp and G. S. Rohrer, *The Journal of Physical Chemistry B*, 1998, 102, 3216-3226.

32. A. Fujishima, X. Zhang and D. A. Tryk, *Surface Science Reports*, 2008, 63, 515-582.

33. J. Yu, J. Low, W. Xiao, P. Zhou and M. Jaroniec, *Journal of the American Chemical Society*, 2014, 136, 8839-8842.

34. R. Gottesman, S. Tirosh, H.-N. Barad and A. Zaban, *The Journal of Physical Chemistry Letters*, 2013, 4, 2822-2828.

35. C. Liu, X. Han, S. Xie, Q. Kuang, X. Wang, M. Jin, Z. Xie and L. Zheng, *Chemistry – An Asian Journal*, 2013, 8, 282-289.

36. M. Mrowetz, W. Balcerski, A. J. Colussi and M. R. Hoffmann, *The Journal of Physical Chemistry B*, 2004, 108, 17269-17273.

37. Y. Cong, J. Zhang, F. Chen and M. Anpo, *The Journal of Physical Chemistry C*, 2007, 111, 6976-6982.

38. C. Burda, Y. Lou, X. Chen, A. C. S. Samia, J. Stout and J. L. Gole, *Nano Letters*, 2003, 3, 1049-1051.

39. J. Hensel, G. Wang, Y. Li and J. Z. Zhang, *Nano Letters*, 2010, 10, 478-483.

40. A. D. Rakić, A. B. Djurišić, J. M. Elazar and M. L. Majewski, *Applied Optics*, 1998, 37, 5271-5283.

41. P. Sudhagar, K. Asokan, E. Ito and Y. S. Kang, *Nanoscale*, 2012, 4, 2416-2422.

42. N. C. Saha and H. G. Tompkins, *Journal of Applied Physics*, 1992, 72, 3072-3079.

43. Y. Nosaka, M. Matsushita, J. Nishino and A. Y. Nosaka, *Science and Technology of Advanced Materials*, 2005, 6, 143.

44. C. Di Valentin, E. Finazzi, G. Pacchioni, A. Selloni, S. Livraghi, M. C. Paganini and E. Giamello, *Chemical Physics*, 2007, 339, 44-56.

45. S.-Y. Du and Z.-Y. Li, *Opt. Lett.*, 2010, 35, 3402-3404.

46. X. Zhang, Y. L. Chen, R.-S. Liu and D. P. Tsai, *Reports on Progress in Physics*, 2013, 76, 046401.

47. A. V. Puga, A. Forneli, H. García and A. Corma, *Advanced Functional Materials*, 2014, 24, 240-240.

48. H. Tada, T. Mitsui, T. Kiyonaga, T. Akita and K. Tanaka, *Nat Mater*, 2006, 5, 782-786.

49. Y. Sun, Z. Sun, S. Gao, H. Cheng, Q. Liu, J. Piao, T. Yao, C. Wu, S. Hu, S. Wei and Y. Xie, *Nat Commun*, 2012, 3, 1057.

50. Y. Wei, L. Ke, J. Kong, H. Liu, Z. Jiao, X. Lu, H. Du and X. W. Sun, *Nanotechnology*, 2012, 23, 235401.

51. S. Y. Reece, J. A. Hamel, K. Sung, T. D. Jarvi, A. J. Esswein, J. J. H. Pijpers and D. G. Nocera, *Science*, 2011, 334, 645-648.